Quantifying the impact of parameters of chloride-induced reinforcement corrosion on the GPR signal

Tešić, Ksenija; Baričević, Ana; Serdar, Marijana; Gucunski, Nenad

Journal article, Published version
Rad u časopisu, Objavljena verzija rada (izdavačev PDF)
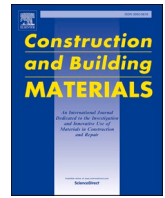
Permanent link / Trajna poveznica: https://urn.nsk.hr/urn:nbn:hr:237:305980

Download date / Datum preuzimanja: **2025-03-14**

Repository / Repozitorij:

Repository of the Faculty of Civil Engineering, University of Zagreb

Quantifying the impact of parameters of chloride-induced reinforcement corrosion on the GPR signal

Ksenija Tesic [a], Ana Baricevic [a,*], Marijana Serdar [a], Nenad Gucunski [b]

[a] *University of Zagreb Faculty of Civil Engineering, Department of Materials, Fra Andrije Kacica-Miosica 26, Zagreb 10000, Croatia*
[b] *Department of Civil and Environmental Engineering, Rutgers, The State University of New Jersey, 500 Bartholomew Road, Piscataway, NJ 08854, USA*

ARTICLE INFO

ABSTRACT

The sensitivity of the high-frequency ground penetrating radar (GPR) signal to changes within the reinforced concrete (RC) makes it a valuable tool for corrosion assessment of RC structures. The most important parameters in chloride-induced corrosion are moisture content, chloride content, and reinforcement diameter loss. The objective of this laboratory study was to investigate and quantify the influence of these parameters on the GPR signal. Of particular interest was to determine which of the observed parameters the GPR is most sensitive to. Furthermore, particular emphasis was placed on understanding the influence of corrosion products, which has not met the consensus in the existing literature. The parameters were studied on a total of forty-two specimens where the reflector of the GPR waves was the reinforcement embedded in the concrete specimen. Based on the experimental data, values of normalized amplitude related to the evaluation of corrosion by GPR were proposed.

1. Introduction

During the initiation phase of chloride-induced corrosion, the main parameters to consider in the inspection of reinforced concrete (RC) structures are moisture and chloride content within the concrete, while in the propagation phase it is a loss of reinforcement cross-section. Unfortunately, in most cases, the parameter that triggers the need for a detailed assessment of RC structures is a visible sign of corrosion on the surface of the structure, e.g., cracks, rust stains, concrete spalling etc. The main reasons for reluctance to perform a detailed assessment in the early stages of corrosion are the duration of the inspection, its complexity and finally the cost. However, the consequences of corrosion [1–5] remind us forcefully on the need of detailed assessment of reinforced concrete structures as part of proactive, rather than reactive infrastructure asset management.

The step towards more efficient maintenance of the RC structures could be the repeated inspection using non-destructive testing (NDT) [6–9]. The main advantages of NDT are more frequent inspection of large areas and shorter inspection time while being completely non-invasive. In recent decades, ground penetrating radar (GPR) has gained importance as a valuable non-destructive testing method in the inspection of structures [10–16]. The analysis of characteristics of electromagnetic waves emitted by the GPR and reflected due to changes

in the interior structure of an element under inspection is of core interest [17,18]. In addition to the wide application of GPR in civil engineering to reconstruct the invisible interior of structural elements [12,19–21], the evaluation of reinforcement corrosion by GPR is of particular interest, but also presents a significant challenge [11,22–27]. Most parameters affecting corrosion of reinforcement in concrete have been previously studied with GPR: moisture content [28–31], chloride content [31–35] and reinforcement corrosion [23,36–40]. While it would be remarkable that one technique could detect all the important parameters affecting the corrosion process, the analysis is more complicated because more than one influential parameter is involved and usually only one outcome parameter is measured, namely the strength of the reflected signal [41–43]. Table 1 gives an overview of laboratory studies on the influence of moisture, chlorides, and corrosion on the GPR signal.

Regarding the reflector, it can be seen from Table 1 that the studies that focused on the moisture/chloride content aimed to show the relationship between the parameters of the concrete and the parameter of the GPR, independently of the corrosion of the rebar. For the corrosion initiation phase, the concrete parameters can be considered independent of the rebar corrosion, but for the corrosion propagation phase, the influence of the corrosion products must be considered. In addition, the effect of corrosion products on the amplitude change is ambiguous and no consensus has yet been reached on whether the corrosion products

2.1.1. Reaching different moisture conditions

Specimens prepared for observation of the effect of moisture on the GPR signal were brought to a saturation level of 15–20%, 45–50%, or 75–80%. A total of nine specimens were prepared for this purpose, three for each saturation range. The specimens were first dried to a constant mass, then saturated to 100%, and finally dried in an oven at 50 °C to the desired degree of saturation. The desired saturation level w was determined according to the following equation,

$$w = (m_3 - m_1)/(m_2 - m_1)\cdot 100 \ [\%] \tag{1}$$

where m_1 is the mass after drying to constant mass, m_2 is the mass after saturation, and m_3 is the mass up to the desired saturation level.

2.1.2. Reaching different chloride-rich conditions

Chlorides were introduced into concrete specimens in two ways, first by adding sodium chloride (NaCl) into the concrete mix (referred to herein as internal chlorides), and second by subjecting the specimens to wet-dry cycles by immersion in sodium chloride solutions, (external chlorides).

A total of 1.19 kg/m³, 1.98 kg/m³, 2.97 kg/m³, 4.95 kg/m³, 9 kg/m³, and 14.94 kg/m³ of sodium chloride were dissolved into potable water and added to the concrete during mixing in the first procedure. The amounts of chlorides correspond to the following chloride concentrations: 0.24%, 0.4%, 0.6%, 1%, 1.8% and 3% of the cement mass, m_c. Eighteen specimens were prepared according to the procedure described above, three for each concentration. All specimens were tested at 0% (dry), 15–20%, 45–50%, 75–80%, and 100% (fully saturated) saturation levels.

The second procedure involved immersing the specimens in a 2%, 3.5%, or 5% sodium chloride solution. The procedure consisted of four cycles of wetting (five days immersion in the solution) and drying (two days drying in the air). Specimens were then immersed until saturation in the same solutions and dried to a saturation level of 0% (dry), 15–20%, 45–50%, and 75–80% and tested with GPR. Three specimens were immersed in each solution, making a total of nine specimens prepared for the described procedure.

2.1.3. Reaching different stages of corrosion

The intended stages of corrosion of the reinforcement in the concrete specimens were achieved by exposing the reinforcement to external current from the laboratory power supply. The specimens had wires for electrical connection that were prepared before casting. The connection between the reinforcement and the wire was protected with an impermeable mastic. On top of the specimens was a container made of polystyrene sheets in which water was placed during the accelerated corrosion process (Fig. 2). The objective was to keep the concrete cover partially wet to force the gradual spread of the corrosion products into the concrete cover. The power supply was set to a voltage of 32 V, but
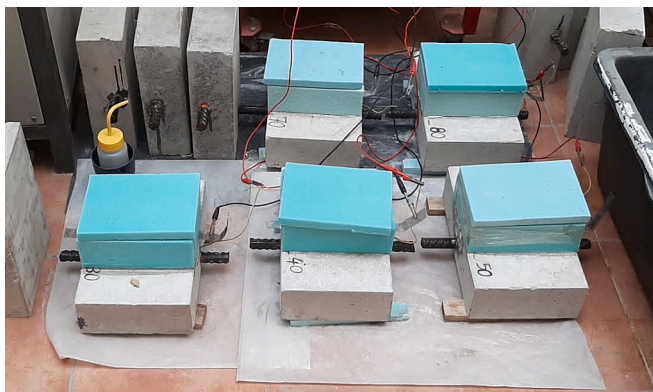
Fig. 2. The setup for the accelerated corrosion process.

with an upper current limit of 0.025 A, corresponding to a current density of 200 μA/cm². A total of six specimens were subjected to the accelerated corrosion process, which differed in the duration of exposure to the external current. The specimens were exposed to the accelerated process for 90, 120, 150, 180, 210, and 240 days. After the accelerated process, the specimens were left under laboratory conditions without a water container for 3 months to stabilize the concrete cover condition, and then the GPR test was performed. The saturation level under laboratory conditions was in the range of 60–65%. This was done to exclude the influence of water content variations in the concrete cover and to ensure that the signal change was only due to the influence of corrosion products.

2.2. GPR measurements

The GPR used in this study was Geophysical Survey Systems Inc. (GSSI) 2.7 GHz device. The scan interval of the instrument was 8 scans/cm, with the scan sampled in 512 data points. The scan range was 5 ns. The scans were processed using RADAN 7 software. The raw GPR data was processed with a bandpass filter and background removal. A constant one-point gain was also used.

GPR profiles were taken from the top of the specimens as shown in Fig. 3. One GPR profile corresponded to the three specimens in a series that came from the same mixture and had the same condition. Two control samples were placed on the sides of the specimens. In addition, a metal plate was placed at the bottom of the series of specimens. The exception was the specimens made for the observation of the influence of the corrosion process, where the profile contained three specimens with different degrees of corrosion between two control specimens. The GPR profiles were taken perpendicular to the reinforcing bars. A total of ten profiles were taken, five forward and five reverse profiles, Fig. 3.

The analysis of the influence of the observed effects on the GPR signal was based on the observation of the peak amplitudes of the signal reflected from the rebar, derived from the scan over the rebar. The amplitudes were extracted, and the final amplitude was determined as the average of ten profiles. The amplitude reported herein is the normalized amplitude A in dB, expressed as:

1) Moisture assessment

$$A = 20\log_{10}(A_m/A_0) \ [dB] \tag{2}$$

where A_m is amplitude at a given saturation level and A_0 is amplitude of the same specimen in dry condition,

2) Chloride assessment

$$A_1 = 20\log_{10}(A_{Cl}/A_0) \ [dB] \tag{3}$$

where A_{Cl} is amplitude at a given chloride concentration and A_0 is amplitude of the specimen without chlorides at the same degree of saturation.

In addition, the influence of chlorides on the GPR signal is expressed by the amplitude A,

$$A = 20\log_{10}(A_{Cl}/A_0) \ [dB] \tag{4}$$

where A_{Cl} is amplitude at a given chloride concentration and A_0 is amplitude of the same specimen in dry condition*.[1]

3) Corrosion assessment

$$A = 20\log_{10}(A_C/A_0) \ [dB] \tag{5}$$

---

[1] For the specimens immersed in the solution, the dry condition was reached before the wet-dry cycles.

Fig. 3. GPR profiles.

where A_C is amplitude at a given stage of corrosion and A_0 is amplitude of the same specimen before corrosion.

It should be mentioned that the values of the amplitudes A_m, A_{Cl}, A_C, and A_0 depend on the particular GPR device and its construction. Also, the values of the amplitudes recorded after propagation through the material 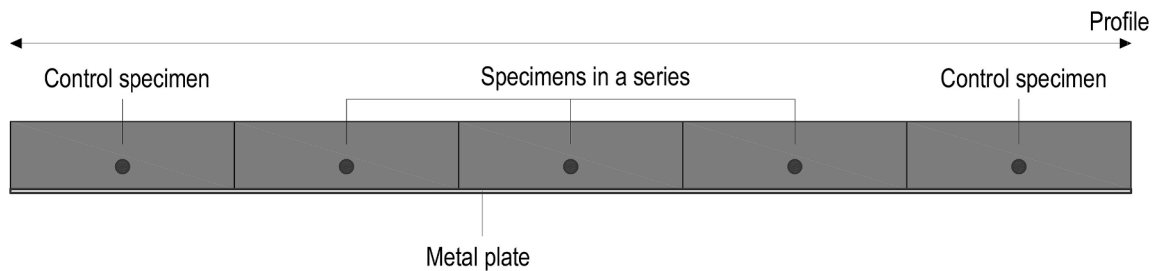depend on the centre frequency of the device. The higher the centre frequency, the greater the attenuation of the signal as it propagates through the same material compared to a device with a lower centre frequency [17]. However, given the normalization procedures (Eqs. (2)–(5)) and the fact that commercially available GPR devices for concrete inspection operate in a similar frequency range, it can be assumed that the results obtained in this work should also apply to investigations other than this particular GPR.

2.3. Chloride profiles

For the specimens prepared for the observation of the influence of chlorides on the GPR signal, the total chloride content was determined by potentiometric titration. The concrete powder was taken every 10 mm to a depth of 50 mm, i.e., to the depth of reinforcement. A known amount of the concrete powder was placed in a beaker and mixed with 100 ml of deionized water and 10 ml of a 5 mol/l nitric acid (HNO_3) solution. The solution was then heated to boiling with constant stirring and stirred for an additional 3 min, according to [49]. The solution was then titrated with 0.1 M silver nitrate ($AgNO_3$). The amount of chlorides is expressed as percentage of the mass of the cement, m_c.

2.4. Reinforcement mass loss

Reinforcement mass loss was measured in the specimens where the effect of corrosion products was observed. All bars were weighed and labelled before mixing the concrete. After the GPR measurements, all specimens were opened at the section where the reinforcement had been placed. After pulling out the reinforcement, the corrosion products were removed mechanically. An angle grinder with a cup brush was used for this purpose. The reinforcement was not additionally cleaned, as it was brought to a metallic gloss by mechanical cleaning. After the corrosion products were removed, the mass of the cleaned rebar was measured. The final mass loss Δm was determined as follows,

$$\Delta m = (m_1 - m_2)/m_1 \cdot 100 \ [\%] \tag{6}$$

where m_1 is the mass of the rebar before concrete mixing and m_2 is the mass of the cleaned rebar after the corrosion process.

3. Results

3.1. Effect of moisture

The normalized amplitude A according to Eq. (2), obtained on a group of specimens where the effect of moisture on the GPR signal was observed is shown in Fig. 4.

The amplitude loss increases with the degree of saturation – the maximum amplitude loss occurs for fully saturated specimens, and according to the normalization to the dry specimen, amplitude A reaches -13.62 dB at a propagation depth of 50 mm. Accordingly, 2.72 dB is lost on each centimetre of concrete when the concrete pores are filled with water. When the pores are half-filled, the loss is one half. This means that the relationship between the normalized amplitude and the degree of saturation can be well expressed in linear terms. However, it was found that larger changes occur at the ends of the saturation range, i.e., below 20% and above 80%. The amplitude loss is related to the mechanisms resulting from the presence of water molecules in the pores of the concrete, i.e., the pore water [50]. When the concrete specimens are exposed to an electromagnetic field, the dipolar molecules tend to
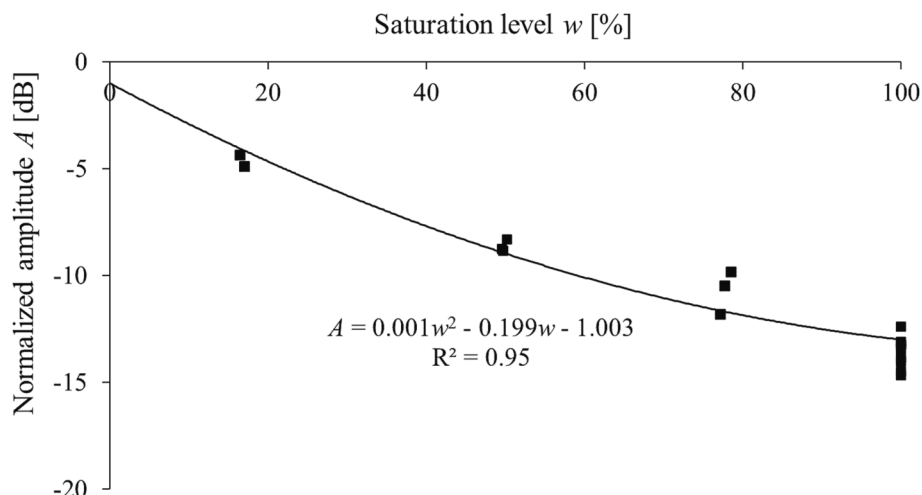

Fig. 4. The normalized amplitude A as a function of the saturation level.

realign according to the applied current and form dipole moments. This effect is called dipolar polarization. As a result of the realignment and the interaction of the particles, some of the energy is converted into heat, leading to an overall decrease in amplitude. The rate of molecular polarization depends on the frequency of the incident pulse [51,52], which means that both the dielectric properties and the amplitude loss are frequency dependent. The behaviour of free water in the presence of an electromagnetic field is described by the Debye model [53]. The Debye diagram shows that there is a relaxation frequency at which the amplitude loss is highest, and this frequency is around 19 GHz for free water molecules. At this frequency, the energy is not transferred for the formation of the organized orientation moments but is consumed in the disordered motion of the molecules. If the water in the material is not completely free to move, as in concrete pores [54,55], the relaxation frequency may fall within the operating range of the GPR, resulting in additional amplitude loss.

3.2. Effect of chlorides

The chloride content, expressed as a percentage of the cement mass, calculated as explained in Section 2.3, is shown in Table 2. Each value in a row in Table 2 is the average chloride content of three specimens.

If the chlorides were added to the concrete during mixing, the chloride profiles in the concrete cover (Table 2) are quite homogeneously distributed for the specimens mentioned. Exceptions are specimens with higher chloride concentration, where the total chloride content is higher near the surface than in the depth of the reinforcement. The reason for this could be the higher water-cement ratio in the first centimetre of the specimens, which is mainly characterised by a higher porosity, thus attracting the higher chloride content [56]. In contrast to the chloride profiles for internal chlorides, the profiles for external profiles tend to show the gradient of the chlorides at the concrete cover. The first centimetre facing the surface that was directly exposed to the sodium chloride solution has the highest concentration, and the concentration decreases with depth.

Fig. 5 shows the normalized amplitude functions according to Eq. (3) as a function of chloride concentration c (mean value in concrete cover). The internal chlorides are marked in black, and the external ones are in magenta. If the amplitude of the reflected wave at a given saturation level for a mixture containing chlorides is normalized to the amplitude of a specimen with the same saturation level but without chlorides (Eq. (3)), the loss can be attributed only to the effect of the chlorides. The positive numbers of A_1 are not included in Fig. 5. The reason for the positive numbers could be slight geometry differences between the two specimens used for normalization, or the position of the rebar in the specimen could influence the described occurrence. This is most pronounced in the examinations at the 15–20% saturation level. This means

that the influence of chlorides is lowest at low saturation levels.

The effect of the chlorides is apparent; it causes amplitude loss. This is mainly the consequence of the increased conductivity of the heterogeneous material [13,50], where the charged ions dissolved in the pore water consume energy in random collisions due to the presence of an electromagnetic field. According to this normalization procedure, the loss for the mixtures with an average chloride content of 0.7% of m_c is –1.6 dB, 1.2% of m_c is –5 dB and 3.1% of m_c is –13.7 dB, all at full saturation. At half saturation, the loss for the mixture with chlorides 3.1% of m_c is –3 dB, while for the mixtures with 0.7% and 1.2% the normalized amplitude has a positive sign according to Eq. (3).

The normalization procedure according to Eq. (4) is intended to show the effect of the amplitude change due to the joint effect of water saturation and chlorides. Fig. 6. shows the behaviour of the amplitude of the GPR signal in accordance with Eq. (4). As for the internal chlorides, the loss is greatest for the mixture with the highest chloride content (3.1 % wt. of cement) and the highest saturation level (100%). The slope of the curves increases with increasing chloride content. At higher saturation levels, the combined effect of water and chlorides is greater because the conduction effects are enhanced by the presence of water due to the facilitated movement of charges in the liquid. In the low saturation range (below 20%), the losses are fairly independent of chloride content. This is probably because the movement of charged ions is restricted in the absence of water. For the mix with an average chloride content of 0.7% of the m_c (internal chlorides group), the signal loss is −14.8 dB for fully saturated specimens. For the concrete with an average chloride content of 1.2% of m_c, the loss is −18.3 dB and for the severe chloride environment with a chloride content of 3.1% of m_c, this loss is −25.6 dB, both at full saturation. For the same mixes, the losses at half-filled pores are −5.6 dB, −7.3 dB and −9.4 dB, respectively. For the specimens with external chlorides, the losses are as follows: −18.2 dB for chloride content of 1.1% of m_c, −22.3 dB for chloride content of 1.6% of m_c and −25.1 dB for chloride content of 2% of m_c, at full saturation, and −11.5 dB, −14.3 dB and −18.3 dB at half saturation.

For the comparison, the specimens to which 1% of chlorides to the m_c was added during mixing (mean chloride content is 1.2% of m_c) and the specimens exposed to a 2% sodium chloride solution (mean chloride content is 1.1% of m_c) have similar average chloride content in the concrete cover. According to Eq. (4), the loss for the first and second groups of specimens is −18.3 dB and −18.2 dB at full saturation and −7.3 dB and −11.5 dB at half saturation. The specimens to which 1.8% of chlorides to the m_c was added and the specimens exposed to a 5% sodium chloride solution have an average chloride content of 1.8% and 2% of m_c, respectively. The losses are as follows: −20.3 dB and −25.1 dB at full saturation and −10.8 dB and −18.3 dB at half saturation. The loss was found to be lower for the internal chlorides than for the external chlorides. This could be explained by the higher ratio of free to total

Table 2
The chloride content in the concrete cover.

Internal chlorides	Chlorides added in mixture [% of m_c]	Chloride concentration [% of m_c]					Mean value	Standard deviation
		Depth [mm]						
		0–10	10–20	20–30	30–40	40–50		
	0.24	0.5	0.4	0.4	0.3	0.4	0.4	0.1
	0.4	0.9	0.7	0.4	0.7	0.5	0.7	0.2
	0.6	0.7	0.6	0.8	0.8	0.6	0.7*	0.1
	1	1.9	1.1	1.1	1.1	0.8	1.2	0.4
	1.8	2.9	1.8	1.4	1.5	1.5	1.8	0.6
	3	5.2	3.1	2.5	2.3	2.6	3.1	1.2
External chlorides	Concentration of solution [%]	Chloride concentration [% of m_c]					Mean value	Standard deviation
		Depth [mm]						
		0–10	10–20	20–30	30–40	40–50		
	2	2.8	1.0	0.6	0.6	0.6	1.1	1.0
	3.5	4.2	1.4	0.9	0.8	0.6	1.6	1.5
	5	4.7	1.7	1.2	1.2	1.1	2.0	1.5

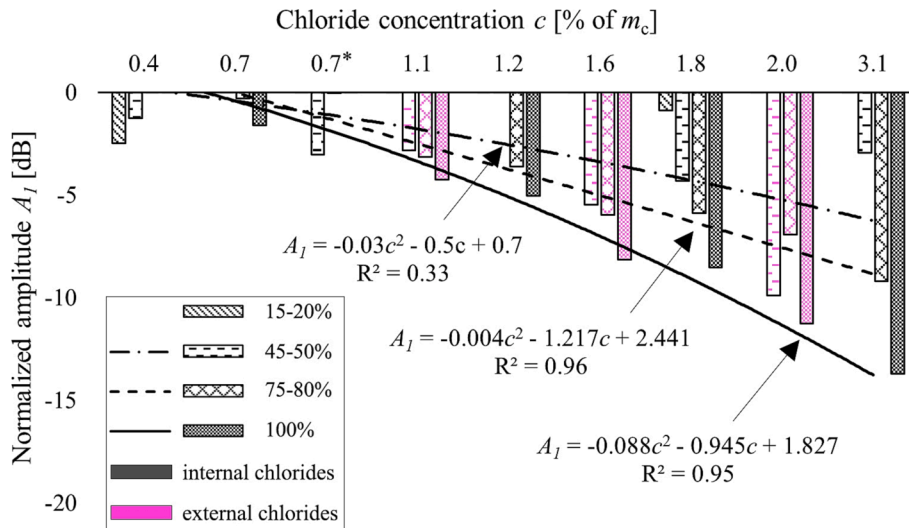* The value that is marked with "*" in Figs. 5 and 6.

Fig. 5. The normalized amplitude A_1 as a function of chloride content.
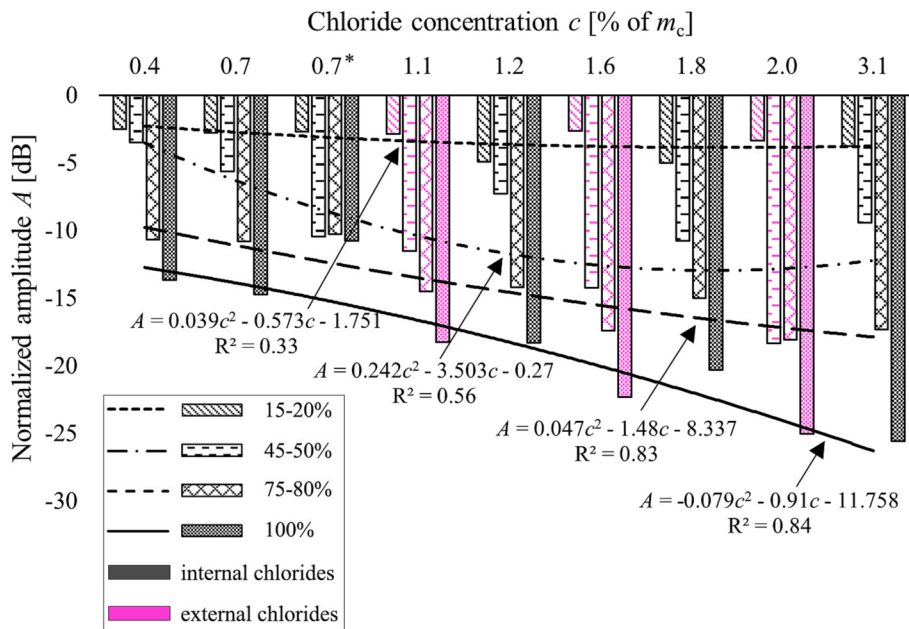

Fig. 6. The normalized amplitude A depending on the average chloride content.

chlorides in the case of the external chlorides [57], which have less restricted motions in the cement matrix compared to the bound chlorides, resulting in higher energy dissipation during particle collision.

3.3. Effect of corrosion products

The signal change due to the corrosion of the reinforcement in the concrete specimen as a function of the mass loss Δm is shown in Fig. 7. The mass loss of the specimens subjected to accelerated corrosion ranges from 0.17% to 2.1%. The main finding of this study is that the increase in corrosion degree affects the amplitude loss. The normalized amplitude according to Eq. (5) ranged from –0.4 dB to –10.8 dB.

For the majority of specimens, the degree of corrosion corresponded to a mass loss between 0.1% and 0.8%. The cross-sections through the corroded reinforcing bars of the specimens opened after completion of the accelerated corrosion process are shown in Fig. 8. It was explained in Section 2.1.3. that the container of water was present during the corrosion process to maintain the concrete cover in a partially wet

condition. In this setup, the ongoing corrosion process and the propagation of the corrosion products develop from the top of the rebar facing the side where the investigation with GPR is performed. This phenomenon was discussed in detail in reference [22]. From Fig. 8, it can be seen that the metal consumption was as explained in the previous sentence. Starting with the lowest corrosion level, the specimens that corroded for 90 days had the smallest corroded area at the top of the rebar. The specimens that corroded for 120, 150, and 180 days had the same but more pronounced corrosion pattern. Finally, the specimens with 210 and 240 days of corrosion, which exhibited the highest degree of corrosion, also had corrosion products on the bottom side of the rebar.

The lowest mass loss is 0.17% and corresponds to an amplitude loss of –0.39 dB. The rebar that corroded for 120 days had a mass loss of 0.46%. The normalized amplitude according to Eq. (5) had a minor value, but with a positive sign. The cross-section of this specimen, shown in Fig. 8, indicates that most of the corrosion products accumulate near the ends of the rebar. On the other hand, most of the radiated GPR energy is reflected from the central part of the rebar, since the profiles
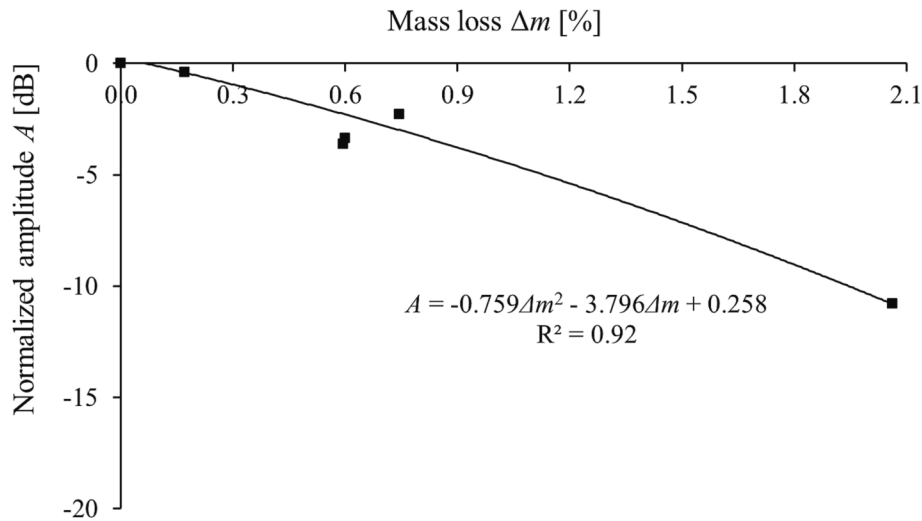
$$A = -0.759\Delta m^2 - 3.796\Delta m + 0.258$$
$$R^2 = 0.92$$

Fig. 7. The normalized amplitude A as a function of corrosion degree.
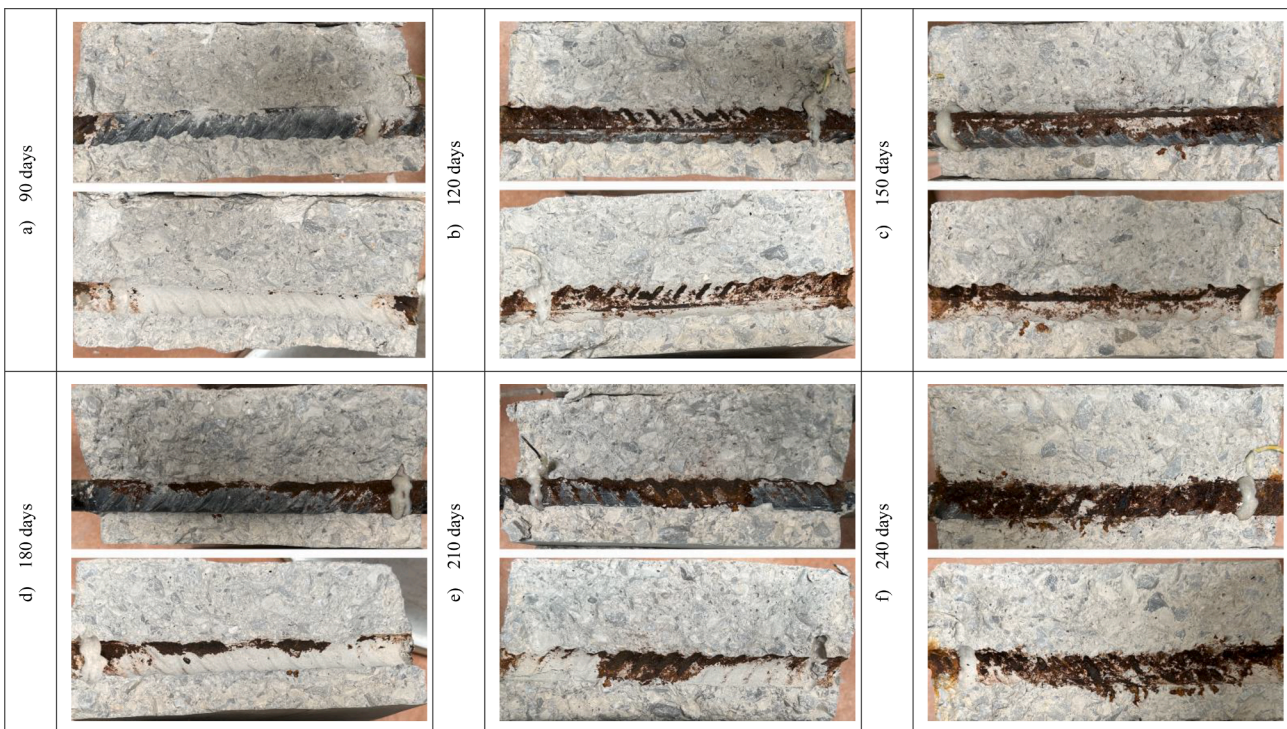
Fig. 8. The cross-section of the corroded specimens after a) 90 days, b) 120 days, c) 150 days), d) 180 days, e) 210 days and f) 240 days of accelerated corrosion.

shown in Fig. 3 correspond to the centreline connecting the specimens. Simplifying the radiated energy as a cone with an ellipse base, as proposed in [58], the central part affected by the electromagnetic waves is the middle 1.5 cm long region of the rebar. The explanation for the lack of amplitude change in this specimen is therefore that the corrosion change did not occur in the central part of the rebar, but on the outer sides of the rebar. The two following specimens, subjected to a corrosion process for 150 and 180 days, had the same degree of corrosion corresponding to a mass loss of 0.6%, so the normalized amplitude had very similar values, –3.6 dB and –3.4 dB, respectively. The specimen with the highest degree of corrosion, i.e., 2.1 % mass loss, had an amplitude loss of –10.8 dB. This specimen had a crack at the end of the corrosion process. However, this crack was less than 1 mm thick, which did not contribute to the overall amplitude change [22,59].

The previously described amplitude loss is probably the result of two mechanisms occurring simultaneously during the propagation of the electromagnetic wave, as described in [22]. The first is the change in the concrete medium in which the wave propagates because the concrete pores are now filled with corrosion products, the iron oxides. Iron oxides have magnetic properties that can affect the amplitude loss [60]. However, this mechanism is not crucial in this study because visible migration of corrosion products toward the concrete cover is not observed (Fig. 8). Instead, the change in amplitude is the result of the change in the reflector surface. The corrosion layer over the rebar changes the reflection coefficient and thus the amplitude of the reflected wave. In addition, the wave is attenuated by the thin corrosion layer during propagation, so the total energy reflected from the steel is lower compared to the uncorroded rebar.

4. Discussion

In Section 3, the loss of GPR signal amplitude was expressed in dB and observed during the propagation of the signal in five centimetres of concrete. In the following discussion, these values are normalised to one centimetre of concrete so that the amplitude is expressed in dB/cm. Table 3 provides an overview of the influence of the corrosion-related effects on the GPR signal. The values of the normalized amplitudes shown in Figs. 4, 5 and 7 are further normalized to the following increase in the observed values: a 5% increase in the saturation level, a 0.4% (of m_c) increase in the total chloride content in concrete cover (mean value for internal and external chlorides) at saturation levels of 45–50%, 75–80%, and 100%, and a 0.1% increase in mass loss due to reinforcement corrosion. It should be mentioned that some of the specimens where the influence of chlorides was observed showed signs of corrosion on the surface of the reinforcing bars (which were detected after opening the specimens), and these were excluded from the analysis of the amplitude in Table 3.

As explained earlier, the changes in signal amplitude due to chlorides are not significant at low saturation ranges, so they are not listed.

It is not easy to select the increment of effects listed in Table 3 to compare their contribution to the overall change in the GPR signal because it is difficult to determine the possible range of effects under real conditions. Even though moisture has a significant effect on the GPR signal, the analysis can be facilitated if the measurement is chosen to avoid variations in the moisture condition. In this case, during the corrosion initiation, chloride contamination has the greatest effect on the signal change for chloride-induced corrosion. Once corrosion progresses, the chlorides and rust simultaneously contribute to the change in signal.

In this work, a dried specimen, or a specimen without chlorides with the same saturation level was used as a reference point for normalization, Eqs. (2) to (4). The normalization provided was used to express the full possible range of amplitude change as a function of specimen moisture conditions, from complete dryness to complete saturation. However, this scenario of extreme conditions is not realistic for most existing reinforced concrete structures. In the maintenance of reinforced concrete structures, the first measurement could be performed on "sound" concrete without deterioration, made after the construction of the structure, as a reference point to which the change in the GPR signal is measured, which indicates changes related to concrete corrosion. If measurements are made under similar environmental conditions, for example, if there has been no rain for several days and average temperatures are similar, extreme variations in the degree of saturation can be avoided.

To determine the value of the amplitude corresponding to the end of the corrosion initiation period, the specimens with a "critical" chloride content of 0.6% of m_c are used [61]. It can be seen from Table 2 that the specimens subjected to wet-dry cycles in 2% and 3.5% sodium chloride solutions have these chloride contents at the reinforcement level. The mean values of the amplitudes are further normalized to the amplitude of a specimen with a moisture content of 3.85% (saturation level 65%), expressed in terms of the mass of the dried specimen. According to [62], this corresponds to an ambient relative humidity of 60%. Finally, the proposed normalized amplitude value that correspond to the critical chloride content of 0.6% of m_c is shown in Table 4.

5. Conclusions

In this experimental study, the influence of moisture, chlorides, and corrosion products on the change of the GPR signal was investigated. The conclusions of this study are:

- Moisture, expressed in this work as saturation level, has strong influence on the GPR signal. However, if the inspection of the structure RC is performed under similar environmental conditions in terms of relative humidity and temperature, this parameter could be excluded from the analysis.
- The corrosion products on the surface of the reinforcement affect the amplitude loss when the signal is reflected. The mass loss of 0.1% affected the amplitude loss of –0.07 dB/cm.
- The normalized amplitude value of –0.7 dB/cm was measured for the specimens where the chloride content at the depth of reinforcement was 0.6% of m_c.

By the proposed reduction of amplitudes for different influencing factors, combined with additional measurements such as chloride content, it is possible to eliminate other factors and analyse the amplitude reduction due to the corrosion process. In addition, in accordance with the procedures described in the paper, the authors would like to emphasise the importance of baseline measurements made shortly after construction. This would open the possibility of using GPR for non-destructive and effective analysis of corrosion of reinforcement in concrete structures. In future studies, the investigations should be extended to different types of concrete in terms of strength so that they can be used for the inspection of structures. In addition, complete structure elements with reinforcement meshes and different reinforcement diameters should also be studied to determine the limits of the inspection.

CRediT authorship contribution statement

Ksenija Tesic: Writing – original draft, Visualization, Methodology, Investigation, Data curation, Conceptualization. **Ana Baricevic:** Writing – review & editing, Supervision, Methodology, Conceptualization. **Marijana Serdar:** Writing – review & editing, Project administration, Funding acquisition, Conceptualization. **Nenad Gucunski:** Writing – review & editing, Supervision.

Declaration of Competing Interest

The authors declare that they have no known competing financial interests or personal relationships that could have appeared to influence the work reported in this paper.

Table 3
Quantification of the influence of corrosion-related effects on the GPR signal.

The corrosion-related effect	Trend of amplitude change		Normalized amplitude [dB/cm]
5% increase in saturation level	↓	At the saturation level 20%–80%	–0.1
		At the saturation level below 20% and above 80%	–0.2
0.4% (of m_c) increase in chloride content	↓	At the saturation level 45–50%	–0.21
		At the saturation level 75–80%	–0.26
		At the saturation level 100%	–0.37
0.1% increase in mass loss due to reinforcement corrosion	↓	At the saturation level 60–65%	–0.07

Table 4
The proposed values of normalized amplitudes for distinguishing passive from active corrosion on an ambient relative humidity of 60%.

Corrosion status	Critical chloride content (of m_c)	Normalized amplitude [dB/cm]
Passive	<0.6	< –0.7
Active	≥0.6	≥ –0.7

Data availability

Data will be made available on request.

Funding

References

[1] M. Domaneschi, C. Pellecchia, E. De Iuliis, G.P. Cimellaro, M. Morgese, A.A. Khalil, F. Ansari, Collapse analysis of the Polcevera viaduct by the applied element method, Eng. Struct. 214 (2020), 110659, https://doi.org/10.1016/j.engstruct.2020.110659.

[2] M. Alexander, H. Beushausen, Durability, service life prediction, and modelling for reinforced concrete structures – review and critique, Cem. Concr. Res. 122 (2019) 17–29, https://doi.org/10.1016/j.cemconres.2019.04.018.

[3] H. Beushausen, R. Torrent, M.G. Alexander, Performance-based approaches for concrete durability: State of the art and future research needs, Cem. Concr. Res. 119 (2019) 11–20, https://doi.org/10.1016/j.cemconres.2019.01.003.

[4] P. Pfändler, K. Bodie, U. Angst, R. Siegwart, Flying corrosion inspection robot for corrosion monitoring of civil structures – First results, in: SMAR 2019 - Fifth Conference on Smart Monitoring, Assessment and Rehabilitation of Civil Structures, SMAR, Potsdam, Germany, 2019, pp. 1–8, https://doi.org/10.3929/ETHZ-B-000365572.

[5] U.M. Angst, Challenges and opportunities in corrosion of steel in concrete, Mater. Struct. Constr. 51 (2018) 4, https://doi.org/10.1617/s11527-017-1131-6.

[6] S. Abu Dabous, S. Feroz, Condition monitoring of bridges with non-contact testing technologies, Automation in Construction 116 (2020) 103224.

[7] M. Solla, B. Riveiro, P. Arias, H. Lorenzo, Introduction, in: B. Riveiro, M. Solla (Eds.), Non-Destructive Techniques for the Evaluation of Structures and Infrastructure, first ed.,, CRC Press, London, 2016, pp. 3–6, https://doi.org/10.1201/b19024.

[8] N. Gucunski, B. Basily, J. Kim, J. Yi, T. Duong, K. Dinh, S.H. Kee, A. Maher, RABIT: implementation, performance validation and integration with other robotic platforms for improved management of bridge decks, Int. J. Intell. Robot. Appl. 1 (2017) 271–286, https://doi.org/10.1007/s41315-017-0027-5.

[9] K. Dinh, T. Zayed, F. Romero, A. Tarussov, Method for analyzing time-series GPR data of concrete bridge decks, J. Bridg. Eng. 20 (2015) 04014086, https://doi.org/10.1061/(ASCE)BE.1943-5592.0000679.

[10] T. Omar, M.L. Nehdi, T. Zayed, Performance of NDT techniques in appraising condition of reinforced concrete bridge decks, J. Perform. Constr. Facil. 31 (2017) 04017104, https://doi.org/10.1061/(asce)cf.1943-5509.0001098.

[11] K. Tesic, A. Baricevic, M. Serdar, Non-Destructive corrosion inspection of reinforced concrete using ground-penetrating radar: A Review, Materials (Basel). 14 (2021) 975, https://doi.org/10.3390/ma14040975.

[12] W.-W.-L. Lai, X. Derobert, P. Annan, A review of ground penetrating radar application in civil engineering: a 30-year journey from locating and testing to imaging and diagnosis, NDT & E Int. 96 (2018) 58–78, https://doi.org/10.1016/j.ndteint.2017.04.002.

[13] K. Dinh, N. Gucunski, J. Kim, T.H. Duong, Understanding depth-amplitude effects in assessment of GPR data from concrete bridge decks, NDT & E Int. 83 (2016) 48–58, https://doi.org/10.1016/j.ndteint.2016.06.004.

[14] K. Dinh, N. Gucunski, K. Tran, A. Novo, T. Nguyen, Full-resolution 3D imaging for concrete structures with dual-polarization GPR, Autom. Constr. 125 (2021), 103652, https://doi.org/10.1016/j.autcon.2021.103652.

[15] K. Dinh, N. Gucunski, Factors affecting the detectability of concrete delamination in GPR images, Constr. Build. Mater. 274 (2021) 121837, https://doi.org/10.1016/j.conbuildmat.2020.121837.

[16] S. Abu Dabous, S. Yaghi, S. Alkass, O. Moselhi, Concrete bridge deck condition assessment using IR Thermography and Ground Penetrating Radar technologies, Autom. Constr. 81 (2017) 340–354, https://doi.org/10.1016/j.autcon.2017.04.006.

[17] D.J. Daniels, Ground penetrating radar, 2nd ed., The Institution of Electrical Engineers, London, 2004.

[18] A.P. Annan, Electromagnetic principles of ground penetrating radar, in: H.M. Jol (Ed.), Ground Penetrating Radar Theory and Applications, Elsevier, Amsterdam, 2009, pp. 3–40, https://doi.org/10.1016/B978-0-444-53348-7.00001-6.

[19] K. Tesic, A. Baricevic, M. Serdar, Comparison of cover meter and ground penetrating radar performance in structural health assessment: case studies, Gradjevinar 73 (2021) 1131–1144, https://doi.org/10.14256/JCE.3323.2021.

[20] V. Pérez-Gracia, F.G. García García, I. Rodriguez Abad, GPR evaluation of the damage found in the reinforced concrete base of a block of flats: A case study, NDT & E Int. 41 (2008) 341–353, https://doi.org/10.1016/j.ndteint.2008.01.001.

[21] V. Perez-Gracia, M. Solla. Inspection procedures for effective GPR surveying of buildings. In: Civil Engineering Applications of Ground Penetrating Radar. Springer: New York, 2015. 97–124. https://doi.org/10.1007/978-3-319-04813-0.

[22] K. Tesic, A. Baricevic, M. Serdar, N. Gucunski, Characterization of ground penetrating radar signal during simulated corrosion of concrete reinforcement, Autom. Constr. 143 (2022), 104548, https://doi.org/10.1016/j.autcon.2022.104548.

[23] S. Hong, W.-W.-L. Lai, G. Wilsch, R. Helmerich, R. Helmerich, T. Günther, H. Wiggenhauser, Periodic mapping of reinforcement corrosion in intrusive chloride contaminated concrete with GPR, Constr. Build. Mater. 66 (2014) 671–684, https://doi.org/10.1016/j.conbuildmat.2014.06.019.

[24] W.-L. Lai, T. Kind, M. Stoppel, H. Wiggenhauser, Measurement of accelerated steel corrosion in concrete using ground-penetrating radar and a modified half-cell potential Method, J. Infrastruct. Syst. 19 (2013) 205–220, https://doi.org/10.1061/(ASCE)IS.1943-555X.0000083.

[25] A. Tarussov, M. Vandry, A. De La Haza, Condition assessment of concrete structures using a new analysis method: Ground-penetrating radar computer-assisted visual interpretation, Constr. Build. Mater. 38 (2013) 1246–1254, https://doi.org/10.1016/j.conbuildmat.2012.05.026.

[26] K. Dinh, N. Gucunski, T. Zayed, Automated visualization of concrete bridge deck condition from GPR data, NDT & E Int. 102 (2019) 120–128, https://doi.org/10.1016/j.ndteint.2018.11.015.

[27] K. Dinh, N. Gucunski, J. Kim, T.H. Duong, Method for attenuation assessment of GPR data from concrete bridge decks, NDT & E Int. 92 (2017) 50–58, https://doi.org/10.1016/j.ndteint.2017.07.016.

[28] S. Laurens, J.P. Balayssac, J. Rhazi, G. Klysz, G. Arliguie, Non-destructive evaluation of concrete moisture by GPR: experimental study and direct modeling, Mater. Struct. 38 (2005) 827–832, https://doi.org/10.1007/BF02481655.

[29] G. Klysz, J.P. Balayssac, Determination of volumetric water content of concrete using ground-penetrating radar, Cem. Concr. Res. 37 (2007) 1164–1171, https://doi.org/10.1016/j.cemconres.2007.04.010.

[30] Z.M. Sbartaï, S. Laurens, J.P. Balayssac, G. Ballivy, G. Arliguie, Effect of concrete moisture on radar signal amplitude, ACI Mater. J. 103 (2006) 419–426, https://doi.org/10.14359/18219.

[31] S.F. Senin, R. Hamid, Ground penetrating radar wave attenuation models for estimation of moisture and chloride content in concrete slab, Constr. Build. Mater. 106 (2016) 659–669, https://doi.org/10.1016/j.conbuildmat.2015.12.156.

[32] J. Hugenschmidt, R. Loser, Detection of chlorides and moisture in concrete structures with ground penetrating radar, Mater. Struct. 41 (2008) 785–792, https://doi.org/10.1617/s11527-007-9282-5.

[33] Z.M. Sbartaï, S. Laurens, J. Rhazi, J.P. Balayssac, G. Arliguie, Using radar direct wave for concrete condition assessment: Correlation with electrical resistivity, J. Appl. Geophys. 62 (2007) 361–374, https://doi.org/10.1016/j.jappgeo.2007.02.003.

[34] A. Kalogeropoulos, J. Van Der Kruk, J. Hugenschmidt, J. Bikowski, E. Brühwiler, Full-waveform GPR inversion to assess chloride gradients in concrete, NDT & E Int. 57 (2013) 74–84, https://doi.org/10.1016/j.ndteint.2013.03.003.

[35] A. Kalogeropoulos, J. Van Der Kruk, J. Hugenschmidt, S. Busch, K. Merz, Chlorides and moisture assessment in concrete by GPR full waveform inversion, Near Surf. Geophys. 9 (2011) 277–285, https://doi.org/10.3997/1873-0604.2010064.

[36] S. Hong, W.-L. Lai, R. Helmerich, Experimental monitoring of chloride-induced reinforcement corrosion and chloride contamination in concrete with ground-penetrating radar, Struct. Infrastruct. Eng. 11 (2015) 15–26, https://doi.org/10.1080/15732479.2013.879321.

[37] V. Sossa, V. Pérez-Gracia, R. González-Drigo, M.A. Rasol, Lab non destructive test to analyze the effect of corrosion on ground penetrating radar scans, Remote Sens. 11 (2019) 2814, https://doi.org/10.3390/rs11232814.

[38] P.T.W. Wong, W.W.L. Lai, J.F.C. Sham, C. Poon, Hybrid non-destructive evaluation methods for characterizing chloride-induced corrosion in concrete, NDT & E Int. 107 (2019), 102123, https://doi.org/10.1016/j.ndteint.2019.05.008.

[39] B.J. Zhan, W.W.L. Lai, S.C. Kou, C.S. Poon, W.F. Tsang, Correlation between accelerated steel corrosion in concrete and ground penetrating radar parameters, in: C. Leung, K.T. Wan (Eds.), international RILEM Conference on Advances in Construction Materials Through Science and Engineering, RILEM Publications SARL, Hong Kong, China, 2011.

[40] R.K. Raju, M.I. Hasan, N. Yazdani, Quantitative relationship involving reinforcing bar corrosion and ground-penetrating radar amplitude, ACI Mater. J. 115 (2018) 449–457, https://doi.org/10.14359/51702187.

[41] ASTM D6087-08. Standard test method for evaluating asphalt-covered concrete bridge decks using ground penetrating radar. https://www.astm.org/d6087-08r15e01.html, 2008. (Accessed 6 March 2023).

[42] M. Abouhamad, T. Dawood, A. Jabri, M. Alsharqawi, T. Zayed, Corrosiveness mapping of bridge decks using image-based analysis of GPR data, Autom. Constr. 80 (2017) 104–117, https://doi.org/10.1016/j.autcon.2017.03.004.

[43] C.L. Barnes, J.-F. Trottier, Effectiveness of ground penetrating radar in predicting deck repair quantities, J. Infrastruct. Syst. 10 (2004) 69–76, https://doi.org/10.1061/(asce)1076-0342(2004)10:2(69).

[44] İ. Kaplanvural, K. Özkap, E. Pekşen, Influence of water content investigation on GPR wave attenuation for early age concrete in natural air-drying condition, Constr. Build. Mater. 297 (2021), 123783, https://doi.org/10.1016/j.conbuildmat.2021.123783.

[45] S.S. Hubbard, J. Zhang, P.J.M. Monteiro, J.E. Peterson, Y. Rubin, Experimental detection of reinforcing bar corrosion using nondestructive geophysical techniques, ACI Mater. J. 100 (2003) 501–510, https://doi.org/10.14359/12957.

[46] A. Zaki, M.A.M. Johari, W.M.A.W. Hussin, Y. Jusman, Experimental assessment of rebar corrosion in concrete slab using ground penetrating radar (GPR), Int. J. Corros. 2018 (2018) 5389829, https://doi.org/10.1155/2018/5389829.

[47] H. Liu, J. Zhong, F. Ding, X. Meng, C. Liu, J. Cui, Detection of early-stage rebar corrosion using a polarimetric ground penetrating radar system, Constr. Build. Mater. 317 (2022), 125768, https://doi.org/10.1016/j.conbuildmat.2021.125768.

[48] S. Hong, GPR-Based periodic monitoring of reinforcement corrosion in chloride-contaminated concrete, Technischen Universität Berlin, Berlin, Germany, 2015.

[49] HZN Standards Publications, HRN EN 14629: 2007, Products and systems for the protection and repair of concrete structures - Test methods - Determination of chloride content in hardened concrete, Croatian Standards Institute, Zagreb, 2007. Accessed 6 March 2023.

[50] N.J. Cassidy. Electrical and magnetic properties of rocks, soils and fluids. In: H.M. Jol (Ed.). Gr. Penetrating Radar Theory Appl., Elsevier, Amsterdam. 2009. 41–72. https://doi.org/10.1016/B978-0-444-53348-7.00002-8.

[51] W.L. Lai, T. Kind, H. Wiggenhauser, Frequency-dependent dispersion of high-frequency ground penetrating radar wave in concrete, NDT & E Int. 44 (2011) 267–273, https://doi.org/10.1016/j.ndteint.2010.12.004.

[52] T. Bourdi, J.E. Rhazi, F. Boone, G. Ballivy, Application of Jonscher model for the characterization of the dielectric permittivity of concrete, J. Phys. D. Appl. Phys. 41 (20) (2008), 205410, https://doi.org/10.1088/0022-3727/41/20/205410.

[53] W.M. Haynes, CRC handbook of chemistry and physics, 97th ed., CRC Press, Boca Raton, 2017.

[54] L. Bertolini, B. Elsener, P. Pedeferri, R.B. Polder, Corrosion of steel in concrete: prevention, diagnosis, repair, Wiley, Weinheim, 2003.

[55] K.S. Cole, R.H. Cole, Dispersion and absorption in dielectrics I. Alternating current characteristics, J. Chem. Phys. 9 (4) (1941) 341–351.

[56] C. Arya, N.R. Buenfeld, J.B. Newman, Factors influencing chloride-binding in concrete, Cem. Concr. Res. 20 (1990) 291–300, https://doi.org/10.1016/0008-8846(90)90083-A.

[57] J. Xu, L. Jiang, W. Wang, Y. Jiang, Influence of CaCl2 and NaCl from different sources on chloride threshold value for the corrosion of steel reinforcement in concrete, Constr. Build. Mater. 25 (2011) 663–669, https://doi.org/10.1016/j.conbuildmat.2010.07.023.

[58] A.P. Annan, S.W. Cosway. Simplified GPR beam model for survey design, in: SEG technical program expanded abstracts 1992. Society of Exploration Geophysicists. 1992. 356–359. https://doi.org/10.1190/1.1822088.

[59] S. Hong, D. Chen, B. Dong, Numerical simulation and mechanism analysis of GPR-based reinforcement corrosion detection, Constr. Build. Mater. 317 (2022), 125913, https://doi.org/10.1016/j.conbuildmat.2021.125913.

[60] N.J. Cassidy, Frequency-dependent attenuation and velocity characteristics of nano-to-micro scale, lossy, magnetite-rich materials, Near Surf. Geophys. 6 (2008) 341–354, https://doi.org/10.3997/1873-0604.2008023.

[61] International Federation for Structural Concrete (fib). Model code for service life design, fib Bulletin No. 34, Lausanne, Switzerland. 2006. ISBN: 2-88394-074-6.

[62] M. Cunningham. When is a concrete slab dry enough? In: Build, April/May, 2008. 25–26. B105–25-DrySlab.pdf, buildmagazine.org.nz. (Accessed 6 March 2023).